

DMD #43273

**EXCRETION, METABOLISM AND PHARMACOKINETICS OF 1-(8-(2-
CHLOROPHENYL)-9-(4-CHLOROPHENYL)-9H-PURIN-6-YL)-4-
(ETHYLAMINO)PIPERIDINE-4-CARBOXAMIDE, CP-945,598, A SELECTIVE
CANNABINOID RECEPTOR ANTAGONIST, IN HEALTHY MALE VOLUNTEERS:**

Zhuang Miao, Hao Sun, Jennifer Liras, and Chandra Prakash
Department of Pharmacokinetics, Dynamics and Metabolism, Pfizer Global Research and
Development, Groton, CT 06340, USA

DMD #43273

Running Title: BIOTRANSFORMATION OF AN ETHYLAMINO-PIPERIDINE-4-CARBOXAMIDE ANALOG

Corresponding Author:

Zhuang Miao

Department of Pharmacokinetics, Dynamics and Metabolism, Pfizer Global Research and Development, Groton, CT 06340, USA

Phone: (860) 287 2591

E-mail address: zhuang.miao@Novartis.com

Abstract: 247

Introduction: 710

Discussion: 1198

Text Pages: 33

Tables: 6

Figures: 10

References 35

Abbreviations: CB-1, cannabinoid type 1; CP-945,598, 1-(8-(2-chlorophenyl)-9-(4-chlorophenyl)-9H-purin-6-yl)-4-(ethylamino)piperidine-4-carboxamide; M1, 4-amino-1-(8-(2-chlorophenyl)-9-(4-chlorophenyl)-9H-purin-6-yl)piperidine-4-carboxamide; ECS, endocannabinoid system; CYP, cytochrome P450; TRA ; total radioactivity ; radio-HPLC, HPLC with on-line radioactivity detector; LC-MS/MS, liquid chromatography-tandem mass spectrometry; β -RAM, radioactive monitor; CID, collision induced dissociation; LSC, liquid scintillation counting; ARC, accurate radioisotope counting

DMD #43273

ABSTRACT

The disposition of 1-(8-(2-chlorophenyl)-9-(4-chlorophenyl)-9H-purin-6-yl)-4-(ethylamino)-piperidine-4-carboxamide (CP-945,598), an orally active antagonist of the cannabinoid CB-1 receptor, was studied following a single 25 mg oral dose of [^{14}C]CP-945,598 to healthy human subjects. Serial blood samples and complete urine and feces were collected up to 672 h postdose. The mean total recovery of radioactivity was 60.1 ± 12.8 from the urine and feces, with majority of dose excreted in the feces. The absorption of CP-945,598 in humans was slow with T_{\max} at 6 h. Less than 2% of the dose was recovered as unchanged drug in the combined excreta, suggesting that CP-945,598 is extensively metabolized. The primary metabolic pathway of CP-945,598 involved N-de-ethylation to form an N-desethyl metabolite (M1), which was then subsequently metabolized by amide hydrolysis (M2), N-hydroxylation (M3), piperidine ring hydroxylation (M6) and ribose conjugation (M9). M3 was further metabolized to oxime (M4) and keto (M5) metabolites. M1, M4 and M5 were the major circulating metabolites, with $\text{AUC}_{(0-48)}$ values 4.7-, 1.5- and 1.1- fold greater than that of CP-945,598. M1, M2 and M9 accounted for 5.6, 33.6 and 6.30% of the dose, respectively, in excreta. The results from *in vitro* experiments with recombinant isoforms suggested that the oxidative metabolism of CP-945,598 to M1 is catalyzed primarily by CYP3A4/3A5. The molecular docking study showed that the N-ethyl moiety of CP-945,598 can access to the heme iron-oxo of CYP3A4 in an energetically favored orientation. Taken together, these data suggest that CP-945,598 is well absorbed and eliminated largely by CYP3A4/3A5-catalyzed metabolism.

DMD #43273

Introduction

Obesity is one of the most serious medical problems of the developed world with over 1.6 of the adult population in the United States alone being overweight or obese. Overweight and obese people carry a higher risk for a variety of cardiovascular diseases including hypertension, coronary heart disease, stroke and peripheral occlusive artery disease, type 2 diabetes and cancer. Due to the rising prevalence of obesity and its ramifications, several drugs including serotonin and noradrenaline inhibitors, lipase inhibitors, B3-adrenoreceptor agonists, leptin agonists, and melanocortin-3 agonists have been developed. However, their use has been limited due to the presence of adverse events and patients' inability to retain weight loss after discontinuation of the therapy.

It has now been well established that the endocannabinoid systems (ECS) play a key role in energy homeostasis by modulating both food intake and peripheral energy metabolism (Patcher et al., 2006; Pagotto et al., 2006; Nogueiras et al., 2009; Akbas et al., 2009). In animals, the stimulation of ECS influences metabolic pathways that lead to weight gain, dyslipidemia, hepatic steatosis, and insulin resistance through cannabinoid type 1 (CB1) receptor activation in brain and peripheral organs (Richard and Boisvert, 2006; Kirkham, 2005; Di Marzo and Matias, 2005). Blockade of the CB1 receptor decreases food intake and induces weight loss in mouse and rat (Arnone et al., 1997; Colombo et al., 1998; Hildebrandt et al., 2003; Vickers et al., 2003; Wiley et al., 2005; Di Marzo and Matias, 2005; Kunos and Tam, 2011). Therefore, CB1 receptor antagonists may be useful as anorectic drugs for the management of obesity and metabolic disease (Di Marzo, 2008; Kunos and Tam 2011).

DMD #43273

CP-945,598, 1-(8-(2-chlorophenyl)-9-(4-chlorophenyl)-9H-purin-6-yl)-4-(ethylamino)piperidine-4-carboxamide, is a selective, high affinity and competitive CB-1 receptor antagonist that inhibits both basal and cannabinoid agonist-mediated CB-1 receptor signaling *in vitro* and *in vivo* (Haddock et al., 2010) and was progressed into Phase 3 human clinical trials as an oral agent for the treatment of obesity (Griffith et al., 2009; Ragan et al., 2009; Haddock et al., 2010). It reduces acute food intake in rodents, decreases food intake and body weight in obese Beagle dogs and humans, and acutely stimulates energy expenditure in rats (Haddock et al., 2010).

The results from pharmacokinetics studies in rats and dogs suggested that CP-945,598 is well absorbed with a bioavailability of 32 to 60% and readily distributed throughout the body. Absorption, distribution, metabolism, and excretion studies with [^{14}C]CP-945,598 in the mouse, rat, and dog resulted in good recovery of the radiolabeled dose, ranging from 98% in rat and mouse to 99% in the dog. The major route of excretion in all three species was via the biliary-fecal route. CP-945,598 is metabolized extensively in all three species since no unchanged parent compound was detected in the urine across species and metabolism was the primary route of clearance (Miao et al., 2011). The primary metabolic pathway was due to the oxidative N-deethylation to form an N-desethyl metabolite (M1), which was then subsequently metabolized to numerous novel and unusual metabolites. In humans, orally administered CP-945,598 is absorbed at a moderate rate ($T_{\text{max}} \sim 4\text{-}6\text{ h}$) and has a terminal phase $T_{1/2}$ of 107-163 h. The metabolic pathways of a drug candidate must be determined in humans to ensure that the all major human circulating metabolites have adequate coverage in preclinical species used for long-term safety evaluation studies (Baillie et. al., 2002). Recently, the Food and Drug

DMD #43273

Administration (FDA) and ICH suggested that additional toxicological testing on metabolites that have higher exposure in humans than preclinical species may be required (Food and Drug Administration, 2008, ICH, 2009). The objectives of the present study were to characterize the disposition of CP-945,598 in healthy obese male volunteers and to identify and quantify its excretory and circulating metabolites. A single dose of [^{14}C]CP-945,598 was orally administered to five human subjects. The urine, feces and serum were collected and assayed for radioactivity, and profiled for metabolites. The metabolites were separated on a reverse phase HPLC system and analyzed by LC/MS and LC/MS/MS, and where possible, the proposed structures were supported by comparisons of their HPLC retention times and MS spectra with those of synthetic standards. Attempts were also made to determine the CYP enzyme responsible for the formation of major metabolites using human liver microsomes, recombinant CYP enzymes and molecular docking.

DMD #43273

Materials and Methods

General Chemicals. Commercially obtained chemicals and solvents were of HPLC or analytical grade. Kromasil C-18 and Luna C-18 analytical columns were obtained from Phenomenex (Torrance, CA). Ecolite (+) scintillation cocktail was obtained from ICN (Irvine, CA). Carbosorb and Permafluor E+ scintillation cocktails were purchased from PerkinElmer Life and Analytical Sciences (Boston, MA). HPLC grade acetonitrile, methanol and water, and certified ACS grade ammonium formate and formic acid were obtained from Fisher Scientific Company (Springfield, NJ).

Radiolabeled Drug and Reference Standards. [^{14}C]CP-945,598 HCl, labeled at the C-8 position of the purinyl moiety (Fig. 1) was synthesized by the radiochemistry group at Pfizer Global Research and Development (Groton, CT) using a standard procedure. It had a specific activity of 3.73 $\mu\text{Ci}/\text{mg}$ free base equivalent and showed a radiochemical purity of >99%, as determined by HPLC using an in-line radioactivity detector. The synthetic reference compounds standards, 4-amino-1-(8-(2-chlorophenyl)-9-(4-chlorophenyl)-9H-purin-6-yl)piperidine-4-carboxamide (CE-156,706, M1), 4-amino-1-(8-(2-chlorophenyl)-9-(4-chlorophenyl)-9H-purin-6-yl)piperidine-4-carboxylic acid (CE-114,764, M2) and 1-(8-(2-chlorophenyl)-9-(4-chlorophenyl)-9H-purin-6-yl)piperidin-4-one (CE-127,773, M5) were synthesized as described earlier (Fig. 1) (Miao et al., 2011).

Human liver microsomes were obtained from Xenotech (Lenexa, KS) and stored at -70°C until used. HL-mix 13 was prepared by mixing liver microsomes from several donors to represent the CYP in normal human. Recombinant human CYP isoforms (CYP1A1, CYP1A2, CYP2C8,

DMD #43273

CYP2C9, CYP2C19, CYP2D6, CYP2E1, CYP3A4 and CYP3A5) were purchased from Gentest (Bedford, MA). The microsomal protein was assayed using BCA assay kit (Pierce, Rockford, IL) and its P450 contents were determined by the method described previously (Omura and Sato, 1964). β -Nicotinamide Adenine Dinucleotide Phosphate (reduced) was purchased from MP Biomedicals Inc. (Aurora, OH).

Subjects and Dose Administration

Five healthy obese male subjects between the ages of 23 to 45 years participated in the study. Three subjects were African Americans, one was mixed of African American and Latino (3-1004) and one subject (5-1009) was the Caucasian. All subjects provided written, informed consent prior to participation in the study. The study protocol, consent documents, consent procedures and subject recruitment procedures were approved by the Independent Institutional Review Board. The study was conducted in compliance with the International Conference on Harmonization (ICH) Good Clinical Practices (GCP) guidelines, the ethical principles that have their origin in the Declaration of Helsinki, and in compliance with the US Food and Drug Administration regulations for informed consent and protection of patient rights. The subjects entered the Clinical Research Facility (DaVita Clinical Research, Minneapolis, MN) 12 h before dosing, and remained there for up to 672 h after dosing under continuous medical observation. All subjects had fasted at least 10 h and were given a single 25 mg oral dose of [^{14}C]CP-945,598 (~94 μCi /subject). The dosing solution was prepared by dissolving the radiolabelled drug in water (100 mL). The drug was administered in an open fashion as a single oral dose in the morning. A standard meal was provided 4 h later. Subjects were required to refrain from lying down during the first four h after drug administration. Subjects were prohibited to consume

DMD #43273

caffeine-containing foods and/or beverages for 24 h prior to dosing and for 48 h after dosing. Administration of the study drug by or under the supervision of medical personnel ensured adherence.

Sample Collection and Storage

Each subject emptied their bladder and provided a 50-ml sample of urine immediately prior to dosing, which was frozen at or below -20 °C. After dosing, urine samples were collected at 24-h intervals for up to 528 h for subject 1-1001, 624 h for subjects 2-1002 and 4-1007, 696 h for subject 3-1004 and 648 h postdose for subject 5-1009. All of the urine collected during each time period was mixed, the total volume recorded, and an aliquot removed for storage at or below -20 °C until analysis. Fecal samples were collected as passed for up to 552 h for subjects 1-1001 and 2-1002, 672 h for subject 3-1004, 624 h for subject 4-1007 and 600 h postdose for subject 5-1009. At the end of study, all subjects had met preset release criteria; approximately 90% of the administered radioactivity was recovered from the urine and feces or 24 hour urine and fecal from 2 consecutive days had radioactivity level of less than 1% of the total administered radioactivity. Venous blood samples (~ 17 mL) for CP-945,598 concentrations and total radioactivity were collected from each subject in glass vacuum blood collection tubes prior to dosing (0) and at 1, 2, 4, 6, 24, 48, 96, 120, 168, 336 and 504 h postdose. For the analysis of CP-945,598 metabolites, venous blood samples (~45 mL) were collected from each subject as described above at 2, 4, 12 and 24 h postdose administration. All blood samples centrifuged and serum samples were collected in separated clean tubes. All these samples were stored at or below -20 °C until analyzed.

Measurement of Total Radioactivity in Serum, Urine and Feces

DMD #43273

All measurements of total radioactivity were performed by liquid scintillation counting (LSC). Samples of serum (500-4000 μ L in duplicate) and urine (~500 μ L in triplicate) from each sampling time point were added to 10-15 mL of scintillation cocktail and counted in a liquid scintillation counter (Beckman, Fullerton, CA).

Fecal samples were transferred into tarred stomacher 3500 bags, hydrated with water (1:4; w/v), and homogenized using a Stomacher homogenizer (Cooke Laboratory Products, Alexandria, VA). Triplicate aliquots (~0.500 μ g) of each fecal homogenate were weighed into Combust cones[®], air dried, and combusted in an oxidizer equipped with a Packard Oximate 80 robot (Model 307, Packard, Downers Grove, IL). The liberated $^{14}\text{CO}_2$ was trapped in 9 mL Carbo-Sorb[®]E, diluted with 10 mL Permafluor[®]E+ scintillation cocktail (Perkin-Elmer Life and analytical Sciences, Boston, MA) and counted in a Perkin-Elmer Wallac 1409 liquid scintillation counter (Perkin-Elmer Life and Analytical Sciences). The combustion efficiency of the sample oxidizer was determined by comparing the radioactivity recovered from replicate oxidations of control samples fortified with a known amount of [^{14}C] to that obtained by direct fortification of the Carbo-Sorb[®]/Permafluor[®] trapping solution with the same amount of [^{14}C]. LSC data (dpm) were automatically corrected for counting efficiency using an external standardization technique and instrument stored quench curve generated from a series of sealed quench standards in Ultima-Gold[™] or Carbo-Sorb[®]/Permafluor[®] cocktails. Radioactivity less than twice the background value was considered to be below the limit of determination. Fecal samples collected prior to dosing were used as the control samples and provided the background count rate.

DMD #43273

The actual dose of radioactivity administered to each subject was determined by measuring the residual radioactivity in the dosing container following dose administration and subtracting this from the total radioactive dose in the dosing container. When determining the amount of radioactivity excreted in urine and feces at each time point as a proportion of the amount administered, the net radioactivity in the actual dose was considered to be 100%. The amount of radioactivity in serum at each time point was calculated using the specific activity of the dose administered and was expressed as nanogram-equiv of parent drug per milliliter.

Extraction of Metabolites from Biological Samples

Urine samples were pooled from 0-384 h for each subject in proportion to the volume of samples collected at different collection interval, the radioactivity in sample pool represented ~91% of total radioactivity excreted in urine, respectively. To remove the urine sediments, 50 mL of pooled urine sample was filtered through a syringe filter disc (Acrodisc Syringe Filter, 25 mm, 1 μ , glass fiber disk, 10 mL of urine per disk). The urine filtrate was loaded onto a preconditioned SPE cartridge (Isolute C8, 5 gm, 25 mL), then eluted with 15 mL of methanol, followed by additional 15 mL of 0.5% ammonium hydroxide in acetonitrile. The elution solvents were then combined and 0.5 mL aliquot was counted by LSC to determine the extraction efficiency. The mean recovery was approximately 88%. The elution solvent was evaporated under nitrogen at 35°C to dryness in a Turbo Vap evaporator (Zymark Corp., Hopkinton, MA). The residue was reconstituted with 0.8 mL of methanol, vortexed and centrifuged for 5 min at 14,000 rpm. The recovery of radioactivity in the final solution after reconstitution was >90%. An aliquot (100 μ L) of the supernatant was injected onto HPLC column and analyzed by a LC-ARC system (AIM Research Company, Hockessin, DE).

DMD #43273

Fecal homogenates were pooled up to 504 h in proportion to the amount of samples collected at different collection intervals to represent approximately 92% of total radioactivity excreted in feces. Pooled fecal sample (40 g) was transferred to a 500 mL Erlenmeyer flask that contained 200 mL of acetonitrile, and then the flask was sonicated for 15 min and vigorously shaken in a 37°C water bath for 3 h. The sample mixture was allowed to settle and the supernatant was filtered into a clean flask. The remaining residue was extracted with additional 140 mL of 0.5% ammonium hydroxide in acetonitrile. The filtrates were combined and 1 mL aliquot was counted for radioactivity by LSC. The mean extraction recovery was estimated to be 89%. The organic solvent was evaporated to dryness under the nitrogen in a Turbo Vap evaporator. The residue was reconstituted with 5 mL of methanol and aliquot of 50 µL was injected onto HPLC column and analyzed by a LC-ARC system.

Serum samples (9-14 mL) at 4, 12 and 24 h post dose from each subject were added dropwise to 80 mL of acetonitrile, vortexed, sonicated for 30 min, and the mixtures were vigorously shaken in a 37°C water bath for 1 h. After centrifugation, the supernatants were separated into the clean 50 mL Falcon polypropylene conical tubes. The pellets were extracted with additional 50 mL of acetonitrile containing 0.5% ammonium hydroxide. Serum samples at 48 h post dose for 5 subjects were pooled together (~1 mL from each subject) and extracted twice with 15 mL of acetonitrile following the aforementioned procedure. The supernatants were combined and aliquots (1 mL) were quantified by LSC. The recoveries were determined to be 84, 93, 91 and 79% for serum samples at 4, 12, 24 and 48 h post dose, respectively. The supernatants were evaporated to dryness under nitrogen in a Turbo Vap evaporator. The residues were then

DMD #43273

reconstituted with 0.4 mL of DMSO: H₂O mixture (1:1) and analyzed by LC-ARC. The serum samples at 48 h from all subjects were pooled by volume and analyzed in a similar way.

***In vitro* Studies of CP-945,598 Metabolism**

Human Liver Microsomes and Recombinant Human CYPs Incubations

Human liver microsomes and recombinant CYP isoforms were reconstituted in 100 mM potassium phosphate buffer (pH=7.4). [¹⁴C]CP-945,598 (10 μM, 0.15 μCi of radiocarbon) was pre-incubated with microsomes (0.5 μM P-450) or recombinant enzyme (20 pmol/mL) for 3 min at 37 °C in a shaking water bath. The incubation was initiated with the addition of 100 μL cofactor (1 mM NADPH, 10 mmol MgCl₂) per 1 mL of incubation mixture. After 60 min, the incubations were terminated by the addition of 4 volumes of acetonitrile to the incubation mixture. The mixture was vortexed for 15 min and centrifuged at 2200 rpm for 15 min. The supernatant was transferred to a clean test tube and evaporated to dryness under stream of nitrogen in a 37°C water bath. The residue was reconstituted with 250 μL of 25% acetonitrile in water. Aliquots (50 μL) were injected onto the HPLC.

Quantitative Assessment of Metabolites

Metabolite quantification from urine, feces and serum was performed by measuring the areas of individually separated HPLC peaks detected using LC-ARC system (AIM Research Company, Hockessin, DE). The LC-ARC system was operated at a stop-flow mode with a 1.2 mL liquid flow cell. The counting time was 60 sec for each 20 sec fraction.

DMD #43273

Metabolite quantification from *in vitro* incubations was performed using a β -RAM (IN/US) and Laura program Version 3.1.1.39 (Lab logic System Ltd). The β -RAM provided integrated peak representation in CPM as well as the percentage of total radioactivity comprised by the each peak within the radiochromatogram. The β -RAM was operated in the homogeneous liquid scintillation counting mode with the addition of 3 mL/min of Tru-Count (IN/US) scintillation cocktail to the HPLC effluent.

High Performance Liquid Chromatography (HPLC)

The HPLC system consisted of a HP-1100 quaternary solvent delivery pump, a HP-1100 membrane degasser, an HP-1100 autoinjector, a HP-1100 photodiode array detector (Hewlett Packard; Palo Alto, CA) and an IN/US radioactive monitor (β -RAM). Chromatography was performed on a Kromasil C-18 column (5 micron, 4.5 x 150 mm) with a mobile phase containing a mixture of 5 mM ammonium formate (pH=3.0) (solvent A) and acetonitrile (solvent B). The mobile phase was initially composed of solvent A/solvent B (80:20). The mobile phase composition was then linearly programmed to solvent A/solvent B (65:35), over 35 min and then changed to solvent A/solvent B 60:40 over 5 min. A gradient was programmed to solvent A/solvent B (20:80) over 10 min and 10:90 over 2 min. The mobile phase composition was returned to the starting solvent mixture over 1 min. The system was allowed to equilibrate for approximately 7 min before making the next injection. The flow rate was 1.0 mL/min and the separation was achieved at ambient temperature.

For serum, four consecutive injections (100 μ L each, 0.5 min apart) were made onto the column to accomplish one profiling analysis. During the first three injections, the HPLC system was

DMD #43273

operated at a flow rate of 0.2 mL/min with a mobile phase consisting of ammonium formate buffer:acetonitrile (97:3). After the fourth injection, the HPLC system resumed the normal gradient program as described above.

For *in vitro* metabolites, the mobile phase was initially composed of solvent A/solvent B (80:20). The mobile phase composition was then linearly programmed to solvent A/solvent B (60:40), over 30 min and then changed to solvent A/solvent B 50:50 over 8 min. A short gradient was programmed to solvent A/solvent B (20:80) over 2 min. The mobile phase composition was returned to the starting solvent mixture over 3 min. The system was allowed to equilibrate for approximately 7 min before making the next injection. The flow rate was 1.0 mL/min and the separation was achieved at ambient temperature.

LC-MS/MS

Identification of the metabolites was performed on a ThermoFinnigan LTQ ion trap mass spectrometer (Thermo electron, Waltham, MA) operating with electrospray (ESI). The effluent from the HPLC column was split and ~50 μ L/min was introduced into the API interface. The remaining effluent was directed to the flow cell of β -RAM. The β -RAM response was recorded in real time by the mass spectrometer that provided simultaneous detection radioactivity and mass spectrometry data. The interface was operated at 5000 V and the spectrometer was operated in the positive ion mode with capillary temperature set at 250°C. Mass spectrometric data analysis was performed using Xcalibur v.1.4 vSR1 (Thermo electron, Waltham, MA).

Pharmacokinetic Analysis

Serum concentrations of CP-945,598 and CE-156,706 (M1) were determined at PPD Development (Richmond, VA) using a validated LC/MS/MS assay (Miao et al., 2011).

DMD #43273

Pharmacokinetic parameters were determined using the WinNonlin Ver. 3.2 program. Maximum observed concentrations (C_{\max}) of CP-945,598, M1 or total radioactivity (parent drug equivalents) in serum were estimated directly from the experimental data, with t_{\max} defined as the time of first occurrence of C_{\max} . Terminal phase rate constants (k_{el}) were estimated using least squares regression analysis of the Serum concentration-time data obtained during the terminal log-linear phase. Half-life ($t_{1/2}$) was calculated as $0.693/k_{el}$. Area under the Serum concentration-time curve from time 0 to the last time (t) with a measurable concentration ($AUC_{(0-t)}$) was estimated using linear trapezoidal rule. AUC from time t to infinity ($AUC_{(t-\infty)}$) was estimated as C_{est}/k_{el} where C_{est} represents the estimated concentration at time t based on the aforementioned regression analysis. AUC from time 0 to infinity ($AUC_{(0-\infty)}$) was estimated as the sum of $AUC_{(0-t)}$ and $AUC_{(t-\infty)}$ values.

Molecular and quantum mechanics-based modeling

The chemical structures of CP-945,598 and its desethyl metabolite M1 were generated by Chem3D (CambridgeSoft Corporation, Cambridge, MA) with geometries optimized using the molecular mechanics method MM2. The derived molecular structures were further optimized and computed using the quantum mechanics-based spin-unrestricted B3LYP (Becke three-parameter Lee-Yang-Parr) density functional theory (DFT) method in the Gaussian 09 program package (Gaussian, Inc., Wallingford, CT). The basis set 6-31G**, a split valence basis set with polarization functions added on both heavy atoms and hydrogens, which was found to be a reliable approach to predict the aliphatic carbon hydrogen abstraction by cytochrome P450s (Sun and Scott, 2010; Sun and Scott, 2011), was implemented in this study. The carbon radical

DMD #43273

intermediates formed at the aliphatic carbons of CP-945,598 and M1 were optimized by the same method by removing a hydrogen atom with the activation energy calculated accordingly.

To prepare for the docking input files, the energetically minimized structures of CP-945,598 and M1 by DFT were further modified by AutoDockTools (The Scripps Research Institute, La Jolla, CA). The Gasteiger atomic charges were assigned with flexible torsions defined for CP-945,598 and M1. The protein template was re-calculated based on a series of the X-ray crystallography determined three-dimensional coordinates of CYP3A4 in the Protein Data Bank [PDB code: 1TQN, 1W0E, 1W0F, 1W0G, 2J0D, 2V0M and 3NXU] and Pfizer's Protein Structure Database (Sun et al., 2009a; Sun et al., 2009b; Sun and Scott, 2011). An oxygen atom was added on top of the heme iron at a distance of 1.7 Å to simulate P450 compound I. The template was further modified with polar hydrogens, Kollman partial charges, and solvation parameters added using AutoDockTools. In addition, AutoGrid 4.0 (The Scripps Research Institute) was applied to define the substrate binding space in CYP3A4, a 60 Å × 80 Å × 80 Å cubic regions covering the active site cavity above the heme porphyrin, and to calculate the grids of van der Waals, hydrogen bonding, electrostatic, torsional, and solvation interactions for each ligand atoms. Docking was accomplished on Pfizer's high performance computing Linux clusters using a Lamarckian genetic algorithm in AutoDock 4.0 (The Scripps Research Institute), which searches the globally energetically optimized conformations and orientations of CP-945,598 and M1. A total of 100 million evaluations were performed for each output binding pose, followed by clustering 200 poses by a root-mean-square deviation (RMSD) method. The lowest energy poses in the proximity of heme were chosen for analysis and visualized by PyMOL (Schrödinger, LLC).

DMD #43273

RESULTS

Urinary and Fecal Excretion and Mass Balance

After a single dose of CP-945,598 to human subjects, the majority of the radioactivity was excreted in the feces (Table 1), with a mean total of $46.1 \pm 12.2\%$ (SD) of the radioactivity at 672 h postdose administration. A mean total of $60.1 \pm 12.8\%$ (SD) of the radioactivity was excreted in the urine and feces over a period of 672 h postdose administration. The mean urinary recovery was $14.0 \pm 3.32\%$. The cumulative mean (\pm SD) recovery of administered radioactivity in urine and feces is shown in fig. 2. Excretion of radioactivity via urine and feces continued for a considerable period of time, with $>20\%$ being excreted during the period 168–672 h post dose administration. It was noted that, for the majority of subjects, there were several days when no fecal sample was collected over the duration of collection period.

Pharmacokinetics of CP-945,598, M1 and Total Radioactivity

The mean (\pm SD) concentration-time profiles of CP-945,598, M1 and total radioactivity in serum of humans following oral administration [^{14}C]CP-945,598 are graphically depicted in fig. 3. Following a single oral dose, serum concentrations of CP-945,598, M1 (CE-156,706) and total radioactivity peaked at 6.0, 6.8 and 6.0 h, respectively. The mean (\pm SD) C_{\max} values for CP-945,598, M1 and total radioactivity were 13.6 ± 3.1 , 42.4 ± 6.4 ng/mL and 74.1 ± 9.6 ng-equiv/g, respectively (Table 2). The mean (\pm SD) $T_{1/2}$ values for CP-945,598, M1 and total radioactivity were 159 ± 33.0 , 139 ± 20.4 and 190 ± 18.4 h, respectively. The mean (\pm SD) $\text{AUC}_{(0-504\text{h})}$ values for CP-945,598, M1 and total radioactivity were 778 ± 223 , $3,731 \pm 317$ ng.h/mL and $8,298 \pm 779$ ng equiv.h/g, respectively. The $\text{AUC}_{0-504\text{h}}$ ratios of CP-945,598 to total radioactivity suggest that $>90\%$ of the total circulating radioactivity was attributable to the metabolites (Table 2).

DMD #43273

Quantitative Profiles of [^{14}C]CP-945,598, and Metabolites in Serum and Excreta

Serum. The representative HPLC-radiochromatograms of serum at 4, 12 and 24 h are shown in fig. 4. CP-945,598 and a total of 3 metabolites were detected in the radioprofiles. The relative amounts of [^{14}C]CP-945,598 and metabolites, expressed as percent of total radioactivity, are presented in Table 3. N-Desethyl- (M1) was the major circulating metabolite at all timepoints. Parent drug, M1, M4 and M5 accounted for 12.1, 57.3, 17.9 and 12.6% of the extracted circulating radioactivity over 0-48 h (Table 3).

Urine and Feces. The representative HPLC-radiochromatograms of urine and feces are shown in fig. 5. In addition to CP-945,598, a total of 5 metabolites were detected in the urine and feces. The relative amounts of [^{14}C]CP-945,598 and metabolites, expressed as the administered dose, in excreta are presented in table 4. Amide hydrolysis product, carboxy- metabolite (M2, CE-114, 764) was the major metabolite in both urine and feces and accounted for 5.4% and 30.9% of the administered dose, respectively. The other metabolites M1, M3 and M6 accounted for 6.8, 1.8 and 2.4% of the dose in the combined excreta. Hydroxylamine glucuronide (M17) was detected only in the urine and represented 4.8% of the dose. Ribose conjugate (M9) accounted for 6.3% of the dose and was present only in the feces (Table 4).

Identification of Metabolites

The fragmentation pattern of CP-945,598 standard was studied to facilitate the interpretation of the mass spectra of its metabolites. Its full scan MS displayed a protonated molecular ion ($\text{M}+\text{H}^+$) at m/z 510; an isotopic peak at m/z 512 (ratio of 3:2) was also observed due to the presence of two chlorine atoms in the molecule. The product ion (MS^2) spectrum of m/z 510 showed a peak at m/z 493, which was formed by a loss of ammonia. (Fig. 6A). High resolution

DMD #43273

MS suggested that the prominent ion at m/z 465 resulted from the characteristic loss of the ethylamine as well as the loss of formamide (Data not shown). The fragments at m/z 356 and 368 resulted from the cleavages across the piperidine ring. These ions were the diagnostic ions for the structural elucidation of metabolites.

Metabolite M1. M1 was detected in feces, urine and serum. The protonated molecular ion of M1 was at m/z 482 and an isotopic peak at m/z 484. The diagnostic ions at m/z 356 and 368, similar to those of parent compound, suggested that the dichlorophenyl purine moiety was unchanged. Based on these data, this metabolite was proposed to be a product formed by N-dethylation of the N-ethyl group. M1 had an identical spectrum to that of CE-156,706 synthetic standard.

Metabolite M2. M2 was detected in feces and urine. The protonated molecular ion of M2 was at m/z 483. The odd MH^+ ion suggested the loss of a nitrogen atom from the parent molecule. Its MS^2 and MS^3 spectra showed fragment ions at m/z 356, 368, 393, 410, 422, 436, 438 and 466 (Fig. 6B). The diagnostic ions at m/z 356 and 368, similar to those of parent compound, suggested that the dichlorophenyl purine moiety was unmodified. M2 had an identical spectrum to that of CE-114,764 synthetic standard. Based on these data, this metabolite was proposed to be a product formed by amide hydrolysis of M1

Metabolite M3. M3 was detected in the urine and feces. Its protonated molecular ion at m/z 498, 12 mass units less than parent compound and 16 mass units higher than M1, suggested the single oxygenation to the M1. Its MS^2 and MS^3 spectra showed fragment ions at m/z 356, 368, 453 and 465 (Fig. 7A). The ion at m/z 465 resulted from the loss of a hydroxylamine moiety. The ion at m/z 453 was produced by de-amidation on the piperidine ring. The diagnostic ions at m/z 356 and 368, similar to those of parent compound, suggested that the dichlorophenyl purine moiety

DMD #43273

was unsubstituted. Based on these data, M3 was identified as 1-[9-(4-chloro-phenyl)-8-(2-chloro-phenyl)-9H-purin-6-yl]-4-hydroxyamino-piperidine-4-carboxylic acid amide.

Metabolite M4. M4 was detected only in the serum. The protonated molecular ion of M4 was m/z 453, 57 Da less than the parent compound, suggesting that M4 was a cleaved product. The odd MH^+ ion suggested the loss of a nitrogen atom from the parent molecule. Its MS^2 and MS^3 spectra showed fragment ions at m/z 356, 368, 383, and 435 (Fig 7B). The ion at m/z 435 resulted from the loss of a water molecule. The diagnostic ions at m/z 356 and 368, similar to those of parent compound, suggested that the dichlorophenyl purine moiety was unchanged. Incubation of M5 (CE-127,773) with hydroxylamine in an ammonium acetate buffer (pH=4) produced a substance that had an identical spectrum and a similar retention time on HPLC to that of M4. Based on these data, M4 was identified as 1-[9-(4-chloro-phenyl)-8-(2-chloro-phenyl)-9H-purin-6-yl]-piperidin-4-one oxime.

Metabolite M5. M5 was detected only in the serum. It showed a protonated molecular ion at m/z 438, 72 Da less than the parent compound, suggesting a cleaved product. Its MS^2 and MS^3 spectra showed fragment ions at m/z 329, 339, 356 and 368. The diagnostic ions at m/z 356 and 368, similar to those of parent compound, suggested that the dichlorophenyl purine moiety was unchanged. M5 had an identical spectrum to that of CE-127,773 synthetic standard. Based on these data, M5 was identified as 1-(8-(2-chlorophenyl)-9-(4-chlorophenyl)-9H-purin-6-yl)piperidin-4-one.

Metabolite M6. M6 was detected in feces and urine. The protonated molecular ion of M6 was m/z 498 and an isotopic peak at m/z 500 in the ratio of 3:2, suggesting that two chlorine atoms were present in the molecule. Its MS^2 and MS^3 spectra showed fragment ions at m/z 356, 368, 463, 480, and 481. The ions at m/z 481 and m/z 480 were due to loss of the NH_3 and water,

DMD #43273

respectively. The diagnostic ions at m/z 356 and 368, similar to those of parent compound, suggested that the dichlorophenyl purine moiety was not substituted. Isolated M6 was treated with titanium trichloride, its retention time on HPLC and associated mass were unchanged, suggesting that M6 was not an N-oxide. Based on these data, this metabolite was proposed to be a product formed by hydroxylation of N-desethyl metabolite (M1).

Metabolite M9a. M9a was detected only in the feces. The protonated molecular ion of M9a was m/z 614. Its MS^2 and MS^3 spectra showed fragment ions at m/z 356, 368, 463, 482, 506, 536, 578 and 596. The ions at m/z 596 and 578 resulted from the consecutive losses of H_2O . M9a was generated by reaction of CE-156,706 with D-ribose in 0.1N NaOH overnight in a 50°C water bath. The reaction mixture contained a chromatographic peak that had a same retention time and similar MS^2 and MS^3 spectra as those of M9a. Based on these data, M9a was identified as a ribose conjugate of CE-156,706 (M1).

Metabolite M17. M17 was detected only in the urine. The protonated molecular ion of M17 was m/z 674 and an isotopic peak at m/z 676 in the ratio of 3:2, suggesting that both chlorine atoms were present in the molecule. Its MS^2 and MS^3 spectra showed fragment ions at m/z 356, 368, 422, 436, 453, 465 and 498. The prominent ion at m/z 498 was formed by a characteristic loss (176 Da), suggesting that M17 was a glucuronide conjugate. The MS^3 (m/z 498) spectrum was identical to the MS^2 spectrum of M3, suggested M17 was a glucuronide conjugate of M3. Based on these data, M17 was identified as a glucuronide conjugate of hydroxylamine metabolite, M3.

DMD #43273

Quantitative Profiles of [^{14}C]CP-945,598, and Metabolites in Human Liver Microsomes and Recombinant CYP Enzymes

Representative HPLC-radiochromatograms of CP-945,598 and its metabolites from human liver microsomes and recombinant CYP3A4/3A5 enzymes are shown in fig 8. CP-945,598 and 5 metabolites were detected in the human liver incubations. The percentages of metabolites are shown in Table 5. N-Desethyl- (M1) and hydroxyl amine (M3) were the major metabolites in human liver microsomes. M4, M5 and M6 accounted for 4.0, 2.5 and 2.3% of the total radioactivity. Only M1 was detected in recombinant human CYP3A4 and 3A5. No metabolite was detected in the incubation of CP-945,598 with CYP1A1, CYP1A2, CYP2C8, CYP2C9, CYP2C19, CYP2D6 and CYP2E1 (data not shown).

Structure-based Modeling of CP-945,598 and M1 with CYP3A4

The molecular docking studies showed that the N-ethyl moiety of CP-945,598 especially its methylene carbon can access to the heme iron-oxo in an energetically favored orientation (Fig. 9A), within the active site space of CYP3A4 confined by the helix I, B-C loop, F-G loop and K- β loop. We found the hydrophobic π - π stacking interactions between the pyrimidine ring of CP-945,598 and the side chain of phenylalanine-108 at the B-C loop (~ 3.7 Å), as well as the potential formation of the hydrogen bond between the amide carbonyl group of CP-945,598 and the hydroxyl group of serine-119 at the B-C loop (~ 3.3 Å between two oxygen atoms), juxtapose the methylene carbon over the heme iron-oxo (~ 2.8 Å from the carbon to the iron-oxo). The calculated activation energy of the methylene carbon is 97.24 kcal/mol (Table 6), in a similar range as those previously reported for N-dealkylation reactions (Sun and Scott, 2011).

Thus, this binding pose suggests an N-deethylation pathway, which is indeed the predominant

DMD #43273

metabolic route we observed in our *in vitro* studies. In addition, the mechanism of the M1 formation indicates the methylene hydrogen abstraction may be more favored than the nitrogen electron abstraction, which is restrained by the piperidine ring. The electron-withdrawing of the neighboring amide carbonyl group also increases the oxidation potential of the nitrogen atom.

The chemical reactivity of other aliphatic carbons of CP-945,598 was also calculated, which indicates that the activation energy of the terminal methyl group of the N-ethyl moiety is approximately 11 kcal/mol higher than that of the methylene. In addition, the calculated activation energy of the piperidine carbon hydrogen abstraction was 105.3 and 97.71 kcal/mol (Table 6), but they are not accessible to the heme iron-oxo due to steric hindrance. For example, several hydrophobic residues of I helix prevent the N-ethyl moiety binding further down toward the heme porphyrin to expose the piperidine ring. Put them together, it also suggests that the N-dealkylation should be a major metabolic pathway of CP-945,598 and the methylene hydrogen atom abstraction appears to be the mechanism.

The docking results of M1 suggest both the newly formed terminal amine group (Fig. 9B) and the piperidine ring (Fig. 9C) can access to the heme iron-oxo in energetically favored orientations. The terminal amine heme-access pose (~ 2.6 Å from the amine nitrogen atom to the heme iron oxo) demonstrated similar molecular interactions as observed for CP-945,598, which may indicate a potential nitrogen oxidation pathway. In addition, the DFT calculation of the hydrogen atom abstraction of M1 showed that the piperidine nitrogen-side carbon hydrogen atom is approximately 7 kcal/mol lower than the one at the amide side; however, the steric effects favor the other way.

DMD #43273

DISCUSSION

In this study, we characterized the routes of elimination, metabolism, and excretion mass balance of [^{14}C]CP-945,598 after a single 25 mg oral dose to humans. A radioactivity dose of 100 μCi of [^{14}C]CP-945,598 was selected for this study based on radioactivity dosimetry estimations from the tissue distribution of [^{14}C]CP-945,598 in rats. A major portion of the administered radioactive dose was eliminated via the fecal (~46%) route and urinary elimination accounted for only ~14% of the dose. These results are consistent with data from the preclinical toxicology species, in which CP-945,598 was eliminated mainly in feces also (Miao et al., 2011). However, the total recovery of administered radioactivity in humans was low (60%) in contrast to preclinical species in which the radioactive dose was quantitatively recovered (>97%). The exact reason for the low recovery in humans is not known but it could be due to several reasons. In general, the recovery of radioactive dose in humans for majority of the compounds is found to be lower than the preclinical species (Roffey et al., 2007). In addition, low recoveries of radioactivity have been observed for compounds, which are eliminated primarily via the feces (Roffey et al., 2007). Low recovery of radioactivity in feces could also be probably due to the sporadic nature of collection in this period (no samples for several days) as a reflection of altered bowel function in these subjects. Other reasons of low recovery in human may be due to the long half-life of the total radioactivity (190 h) and/or possible adipose tissue uptake of total radioactivity followed by slow elimination.

Pharmacokinetic analysis of total radioactivity and unchanged CP-945,598 suggested that the absorption was slow as the serum concentrations of both peaked at 6.0 h. Serum concentrations

DMD #43273

of total radioactivity greatly exceeded to those of CP-945,598 at all-time points, indicating that. Systemic exposure ($AUC_{(0-\infty)}$) to total radioactivity in serum was ~ 11 fold greater than the parent compound, CP-945,598, demonstrating that the majority of circulating radioactivity was attributable to metabolites. Based on C_{max} and $AUC_{(0-\infty)}$ values, the exposure of M1 was 3-to 5 – fold higher than the parent drug. The elimination of total radioactivity, CP-945,598 and M1 was also slow as indicated by their long terminal elimination half-lives (190 h for total radioactivity, 159 h for CP-945,598 and 139 h for M1). The mean half-life estimate was appreciably longer for total radioactivity compared with parent CP-945,598 and its major metabolite M1. This observation, together with greater systemic exposure observed for total radioactivity, could not be accounted for by CP-945,598 and the major metabolite M1 alone, it reflects the formation of other radiolabeled metabolites that persist in the circulation longer than the parent compound and M1. In addition, the similar half-life estimates for CP-945,598 and M1 also suggest that this metabolite is formation-rate limited, whereas some other metabolites (associated with total radioactivity) may be elimination-rate limited.

The urine and feces radiochromatograms also indicate that CP-945,598 is extensively metabolized since <1.6% of the administered dose was excreted unchanged in excreta. A total of 8 metabolites were identified by LC-MS/MS (Prakash et al., 2007) and, where possible, the proposed structures were supported by comparison of their HPLC retention times and MS^2/MS^3 spectra with those of the synthetic standards. Based on the structure of metabolites, metabolic pathways of CP-945,598 in humans are shown in fig. 10. The primary metabolic pathway of CP-945,598 involved N-dethylation to form an N-desethyl metabolite (M1), which is then subsequently metabolized by amide hydrolysis to piperidine-4-carboxylic acid (M2), N-

DMD #43273

hydroxylation to hydroxyamino-piperidine-4-carboxamide (M3), piperidine ring hydroxylation to hydroxypiperidine-4-carboxamide (M6) and ribose conjugation to M9. M3 was further metabolized to novel and unusual oxime (M4) and keto (M5) metabolites. The major excretory metabolites were M1 and M2, accounting for 36.3% of the administered dose. Human circulating metabolites included M1, M4 and M5. All three human metabolites (M1, M4, and M5) were each present in serum of the preclinical toxicology species (rat, mice, and dog) (Miao et al., 2011) and each metabolite was present in at least one of the animal species at exposures that were similar to or exceeded the human exposure. The most abundant circulating metabolites M1 was pharmacologically inactive and, therefore, it is not expected to contribute towards the efficacy of the parent drug.

In this study, we identified two oxidative metabolites (M4 and M5) and a ribose conjugate (M9a), similar to those identified in rats and dogs (Miao et al., 2011). Although, similar biotransformation of amino acids has been reported in higher plants (Halkier et al., 1989), the formation of M4 in mammals is novel and to our knowledge has not been reported. It has also been shown that two *Arabidopsis* CYPs, CYP79B2 and CYP79B3 metabolized an important intermediate, indole-3-acetaldoxime, implicated in auxin biosynthesis, by decarboxylation and subsequent dehydrogenation (Halkier et al., 1989; Zhao et al., 2002). Another possibility is via the hydroxylamine and nitron formation pathway, for example, previous study found indoline was biotransformed to an indoline nitron that was tautomerized to produce *N*-hydroxyindole (Sun et al., 2007). It appears that the M4 formation may be initiated from the nitrogen radical cation formation and then the oxygen rebound due to the lack of the vicinal carbon hydrogens,

DMD #43273

followed by the nitron formation and decarboxylation. The exact mechanism and the enzyme(s) involved for the formation of M4 are under investigation at this time.

Incubation of CP-945,598 with human liver microsomes resulted in the formation of five metabolites, M1, M3, M4, M5 and M6, similar to those observed in vivo. Incubation of CP-945,598 with recombinant human CYPs, showed that only CYP3A4 and 3A5 form the major metabolite M1. Other recombinant CYPs demonstrated low or no metabolism of CP-195,543, suggesting that that CP-945,598 is eliminated primarily by CYP3A4/3A5-catalyzed metabolism. The human CYP3A family, accounting for ~50% of the total P450 in human liver, is clinically very important because it has been shown to metabolize a large number of drugs (Wrighton et al 1996). The human CYP3A subfamily includes CYP3A4, CYP3A5, CYP3A7 (Li et al. 1995), and CYP3A43 (Domanski et al., 2001) as sub-family members. CYP3A4 is the major human liver CYP3A enzyme, whereas CYP3A5 is present in only ~10-30% of the human liver and CYP3A7 is only present in fetal liver. CYP3A5*1 is a polymorphic-expressed enzyme in which the allelic frequency of wild-type is only 10 to 15% in the whites and 50% in blacks (Daly, 2006). Although it is not currently possible to make a quantitative extrapolation from recombinant CYP3A5 data because of the lack of an appropriate CYP3A5 probe substrate for the generation of relative activity factors, the low rate of metabolism of CP-945,598 by CYP3A5 compared with CYP3A4 suggests that no dosage adjustment will be needed in populations in which the expression of this polymorphic enzyme is high.

In conclusion, this open-label Phase I study has shown that CP-945,598 is well absorbed, extensively metabolized to multiple oxidative metabolites primarily by P450-dependent

DMD #43273

pathways, and the radiolabeled material is eliminated by the biliary-fecal route. All the human metabolites were present in all animal species used for long term safety and carcinogenicity assessments.

DMD #43273

ACKNOWLEDGEMENTS

We would like to thank Dr Klaas Schildknecht and Mr. Keith T. Garnes for providing radiolabeled CP-945,598.

AUTHORSHIP CONTRIBUTION:

<u>Contribution</u>	<u>Author Name</u>
Participated in research design	Zhuang Miao, Chandra Prakash, Jennifer Liras
Conducted experiments	Zhuang Miao
Performed data analysis	Zhuang Miao, Chandra Prakash, Hao Sun
Wrote or contributed to the writing of the manuscript	Zhuang Miao, Chandra Prakash, Hao Sun

DMD #43273

REFERENCES

- Akbas F, Gasteyger C, Sjödin A, Astrup A, and Larsen TM (2009) A critical review of the cannabinoid receptor as a drug target for obesity management. *Obes Rev* 10: 58–67
- Arnone M, Maruani J, Chaperon F, Thiebot MH, Poncelet M, Soubrie P and Le Fur G (1997) Selective inhibition of sucrose and ethanol intake by SR 141716, an antagonist of central cannabinoid (CB1) receptors. *Psychopharmacology (Berlin)* 132: 104–106.
- Baillie TA, Cayen MN, Fouda H, Gerson RJ, Green JD, Grossman SJ, Klunk LJ, LeBlanc B, Perkins DG, Shipley LA (2002) Drug Metabolites in Safety Testing. *Toxicol Appl Pharmacol* 182: 188-196.
- Colombo G, Agabio R, Diaz G, Lobina C, Reali R, Gessa GL (1998) Appetite suppression and weight loss after the cannabinoid antagonist SR 141716. *Life Sci* 63(8): PL113-PL117
- Daly AK (2006) Significance of the minor cytochrome P450 3A isoforms. *Clin Pharmacokinet* 45:13-31.
- Domanski DL, Finta C, Halpert JR and Zaphiropoulos PG.(2001) cDNA cloning and initial characterization of cYP3A43, a novel human cytochrome P450. *Mol Pharmacol* 59: 386-392
- Di Marzo V and Matias I (2005) Endocannabinoid control of food intake and energy balance. *Nat. Neurosci* 8: 585-589.
- Di Marzo V (2008) CB1 receptor antagonism: biological basis for metabolic effects. *Drug discov Today* 13: 1026-1041
- Food and Drug Administration, *Safety Testing of drug Metabolites*, FDA, Editor. 2008. p. <http://www.fda.gov/CDER/GUIDANCE/6897fnl.pdf>.
- Griffith DA, Hadcock JR, Black SC, Iredale PA, Carpino PA, DaSilva-Jardine P, Day R, DiBrino J, Dow RL, Landis MS, O'Connor RE, Scott DO (2009) Discovery of 1-[9-(4-Chlorophenyl)-8-(2-chlorophenyl)-9H-purin-6-Yl]-4-ethylaminopiperidine-4-carboxylic Acid Amine Hydrochloride (CP-945,598), a Novel, Potent and Selective Cannabinoid CB1 Receptor Antagonist. *J Med Chem* 52: 234-237
- Hadcock JR, Griffith DA, Iredale PA, Carpino PA, Dow RL, Black S, O'Connor R, Gautreau D, Lizano JS, Ward K (2010) In vitro and in vivo pharmacology of CP-945,598, a potent and selective cannabinoid CB1 receptor antagonist for the management of obesity. *Biochem Biophys Research Comm* 394(2): 366-71.
- Halkier BA, Olsen CR and Moller BL (1989) The biosynthesis of cyanogenic glucosides in higher plants. *J. Biol. Chem* 264: 19487-19494

DMD #43273

- Hildebrandt AL, Kelly-Sullivan DM, Black SC (2003) Antiobesity effects of chronic cannabinoid CB1 receptor antagonist treatment in diet-induced obese mice. *Eur. J. Pharmacol* 462: 125–132.
- ICH, *ICH Guidance on Non-clinical Safety Studies for the Conduct of Human Clinical Trials and Marketing Authorization for Pharmaceuticals M3(R2)*. 2009. p.
<http://www.emea.europa.eu/pdfs/human/ich/028695en.pdf>
- Kirkham TC (2005) Endocannabinoids in the regulation of appetite and body weight, *Behav. Pharmacol* 16:297-313.
- Kunos G and Tam, J (2011) The case for peripheral CB1 receptor blockade in the treatment of visceral obesity and its cardiometabolic complications. *Br J Pharmacol* 163(7): 1423-1431.
- Li AP., Kaminsky D L and Rasmussen A, (1995) Substrate of human hepatic cytochrome P450 3A4. *Toxicology* 104:1-8.
- Miao Z, Scott DO, Griffith DA, Day R and Prakash C (2011) Excretion, metabolism and pharmacokinetics of 1-(8-(2-chlorophenyl)-9-(4 chlorophenyl)-9h-purin-6-yl)-4-(ethylamino)piperidine-4-carboxamide, cp-945,598, a selective cannabinoid receptor antagonist, in rats, mice and dogs: species and gender related differences. *Drug Metab Dispos*
doi:10.1124/dmd.111.040360
- Nogueiras R, Diaz-Arteaga A, Lockie SH, Vela'squez DA, Tschöp J, López M, Cadwell CC, Die'guez C, and Tschöp MH (2009) The endocannabinoid system: role in glucose and energy metabolism. *Pharmacol Res* 60: 93–98.
- Omura, T. and Sato, R., (1964) The carbon monoxide binding pigment of liver microsomes. *J Biol Chem* 239: 3137-3142.
- Pagotto U, Marsicano G, Cota D, Lutz B, and Pasquali R (2006) The emerging role of the endocannabinoid system in endocrine regulation and energy balance. *Endocr Rev* 27: 73–100.
- Prakash C, Shaffer C, Nedderman A (2007) Analytical strategies for identifying drug metabolites. *Mass Spectrom Rev* 26: 340-369.
- Ragan JA, Bourassa DE, Blunt J, Breen D, Busch FR, Cordi EM, Damon DB, Do N, Engtrakul A, Lynch D, McDermott RE, Mongillo JA, O'Sullivan MM, Rose PR and Vanerplas C (2009) Development of a practical and efficient synthesis of CP-945598-01, a CB1 antagonist for the treatment of obesity. *Org Proc Res Develop* 13(2): 186-197.
- Richard D and Boisvert P (2006) The endocannabinoid system and its role in energy homeostasis and abdominal obesity management. *Int. Obes* 30: S1-S2.
- Roffey SJ, Obach RS, Gedge JJ, and Smith DA (2007) What is the objective of the mass balance study? A retrospective analysis of data in animal and human excretion studies employing radiolabeled drugs. *Drug Metab Rev* 39: 17–43.

DMD #43273

Sun H and Scott DO (2010) Structure-based drug metabolism predictions for drug design. *Chem Biol Drug Des* 75: 3-17.

Sun H and Scott DO (2011) Metabolism of 4-Aminopiperidine Drugs by Cytochrome P450s: Molecular and Quantum Mechanical Insights into Drug Design. *ACS Med Chem Lett* 2: 638-643.

Sun H, Ehlhardt WJ, Kulanthaivel P, Lanza DL, Reilly CA, and Yost GS (2007) Dehydrogenation of indoline by cytochrome P450 enzymes: a novel "aromatase" process. *J Pharmacol Exp Ther* 322: 843-851.

Sun H, Moore C, Dansette PM, Kumar S, Halpert JR, and Yost GS (2009a) Dehydrogenation of the indoline-containing drug 4-chloro-N-(2-methyl-1-indoliny)-3-sulfamoylbenzamide (indapamide) by CYP3A4: correlation with in silico predictions. *Drug Metab Dispos* 37: 672-684.

Sun H, Sharma R, Bauman J, Walker DP, Aspnes GE, Zawistoski MP, and Kalgutkar AS (2009b) Differences in CYP3A4 catalyzed bioactivation of 5-aminooxindole and 5-aminobenzosultam scaffolds in proline-rich tyrosine kinase 2 (PYK2) inhibitors: retrospective analysis by CYP3A4 molecular docking, quantum chemical calculations and glutathione adduct detection using linear ion trap/orbitrap mass spectrometry. *Bioorg Med Chem Lett* 19: 3177-3182.

Vickers SP, Webster LJ, Wyatt A, Dourish CT, Kennett GA (2003) Preferential effects of the cannabinoid CB1 receptor antagonist, SR 141716, on food intake and body weight gain of obese (fa/fa) compared to lean Zucker rats. *Psychopharmacol (Berlin)* 167: 103-111.

Wiley JL, Burston JJ, Leggett DC, Alekseeva OO, Razdan RK, Mahadevan A, Martin BR (2005) CB1 cannabinoid receptor-mediated modulation of food intake in mice. *Br J Pharmacol* 145(3): 293-300.

Wrighton SA, VandenBranden M, and Ring BJ (1996) The human drug metabolizing cytochrome P450. *J. Pharmacokinetics and Biopharmacology* 24: 461-473.

Zhao Y and Hull AK et al.(2002) Trp-dependent auxin biosynthesis in *Arabidopsis*: involvement of cytochrome P450s CYP79B2 and CYP79B3. *Genes Dev* 16: 3100-3112.

DMD #43273

Footnotes:

Zhuang Miao, Current Address: Novartis, East Hanover, NJ

E-mail address: zhuang.miao@Novartis.com

Chandra Prakash, Current Address: Biogen Idec, Cambridge, MA, 02142

E-mail address: chandra.prakash@biogenidec.com

DMD #43273

Figure Legends

Fig.1. The Structures of [^{14}C]CP-945,598 and synthetic standards

Fig.2. Mean (\pm SD) cumulative recovery of radioactivity after administration of a single 25 –mg oral dose of [^{14}C]CP-945,598 to healthy obese human subjects (n=5).

Fig.3. Mean (\pm SD) serum concentration-time curves for CP-945,598, CE-156,706 (M1) and total radioactivity in healthy obese human subjects (n=5) following a single 25 mg oral dose of [^{14}C]CP-945,598

Fig.4. HPLC-radiochromatograms of CP-945,598 and its metabolites in serum at 4, 12 and 24 h postdose following a single 25 mg oral dose of [^{14}C]CP-945,598

Fig.5. HPLC-radiochromatograms of CP-945,598 and its metabolites in urine (0-384 h) and feces (0-384 h) following a single 25 mg oral dose of [^{14}C]CP-945,598

Fig.6. CID product ion spectra of (A) CP-945,598 (m/z 510) and (B) M2 (m/z 483)

Fig.7. CID product ion spectra of (A) M3 (m/z 498) and (B) M4 (m/z 453)

Fig.8. HPLC-radiochromatograms of [^{14}C]CP-945,598 and its metabolites in (A) human liver microsomes (B) CYP 3A4 and (C) CYP3A5.

Fig.9. Molecular docking poses of CP-945,598 (A) and M1 (B and C) in the active sites of CYP3A4. Conformations and orientations were predicted by AutoDock with the lowest energy binding cluster(s) close to the heme illustrated by PyMOL. CYP3A4 is shown in a cartoon format, with the iron oxo as spheres, and heme (pink), docked

DMD #43273

substrates (cyan for CP-945,598 and yellow for M1) and active site residues (green) as color-coded sticks: red for oxygen, blue for nitrogen and green for chlorine.

Fig.10. Proposed metabolic pathways of CP-945,598 in humans

DMD #43273

Table 1 Total excretion of [^{14}C]CP-945,598-derived radioactivity in excreta of healthy, obese adult male subjects after a single oral administration.

Subject	Urine (0-696 h)	Feces (0-672 h)	Total (0-696 h)
	Percent Administered Dose (%)		
1-1001	11.8	35.8	47.6
2-1002	18.1	37.9	56.0
3-1004	15.7	45.0	60.7
4-1007	9.7	45.2	54.9
5-1009	14.8	66.7	81.5
Mean	14.0	46.1	60.1
SD	3.32	12.2	12.8

DMD #43273

Table 2. Pharmacokinetic parameters of CP-945,598, CE-156,706 and total radioactivity in humans following a single 25 mg oral dose of [¹⁴C]CP-945,598.

Analyte	Subject	T _{max} (h)	C _{max} (ng/mL)	AUC _{0-last} (ng.h/mL)	AUC _{0-∞} (ng.h/mL)	T _{1/2} (h)
CP-945,598	1-1001	6	15.4	633	690	166
	2-1002	6	10.8	517	561	102
	3-1004	6	15.7	1092	1227	174
	4-1007	4	16.3	879	992	187
	5-1009	8	9.79	770	849	165
	Mean±SD	6.0±1.4	14±3.1	778±223	864±260	159±33
M1 (CE-156,706)	1-1001	6	50.0	3443	3651	138
	2-1002	6	46.7	4071	4177	111
	3-1004	6	43.8	4018	4243	129
	4-1007	8	35.9	3741	4087	162
	5-1009	8	35.7	3384	3672	155
	Mean±SD	6.8±1.1	42±6.4	3731±317	3966±284	139±20
Total Radioactivity	1-1001	6	68.4	8219	9127	165
	2-1002	6	88.6	9438	10960	197
	3-1004	4	68.7	7438	8626	201
	4-1007	6	79.0	8623	9352	177
	5-1009	8	65.7	7774	9107	210
	Mean±SD	6.0±1.4	74±9.6	8298±779	9434±893	190±18

DMD #43273

Table 3. Mean (\pm SD) ^{14}C -radioactivity-derived serum concentrations and AUCs of CP-945,598 and its metabolites over 0-48 h.

Time (h)	Concentration ng-equiv/g* \pm SD				AUC	% Total AUC
	4	12	24	48	ng-equiv-h/g	%
Parent	11.5 \pm 9.5	8.0 \pm 2.7	6.4 \pm 2.2	2.7 \pm NA**	297 \pm 99.9	12.1 \pm 4.5
M1	28.4 \pm 5.8	38.1 \pm 4.9	31.8 \pm 2.5	23.1 \pm NA	1401 \pm 99.3	57.3 \pm 2.7
M4	10.1 \pm 6.0	10.9 \pm 4.1	10.9 \pm 4.9	6.0 \pm NA	438 \pm 146.7	17.9 \pm 4.3
M5	4.5 \pm 1.6	3.6 \pm 1.8	7.2 \pm 4.0	9.7 \pm NA	309 \pm 95.7	12.6 \pm 3.0

Serum concentrations (ng-equiv/g) were calculated using the multiple of ^{14}C -derived radioactivity and the extraction recovery corrected % radioactivity detected in HPLC-radiochromatograms.

NA; not available, 48h plasma sample was pooled from each individual due to low radioactivity.

DMD #43273

Table 4 Percentages (mean±SD) of excretory metabolites of CP-945,598 in healthy obese human subjects following oral administration of [¹⁴C]CP-945,598 (urine pooled from 0-384 h)

Metabolite (#)	m/z	% of Dose		
		Urine	Feces	Total
Parent	510	0.2±0.1	1.4±0.9	1.6±0.9
M1	482	2.3±0.6	4.5±0.5	6.8±0.8
M2	483	5.4±1.5	30.9±14.8	36.3±15.5
M3	498	0.6±0.1	1.2±0.6	1.8±0.1
M6	498	0.5±0.1	1.9±0.6	2.4±0.7
M9a	ND	ND	6.3±4.3	6.3±4.3
M17	674	4.8±1.4	ND	4.8±1.4

ND: not detected

DMD #43273

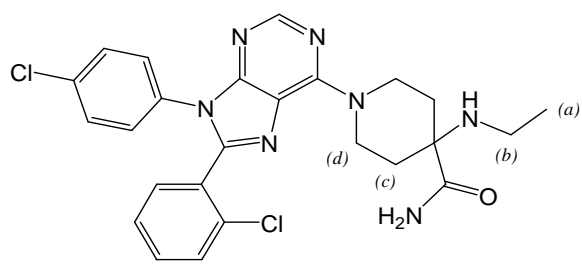
Table 5. Percentage of CP-945,598 metabolites in liver microsomes, CYP3A4 and 3A5

Metabolite #	<i>m/z</i>	RT (min)	Human LM	CYP3A4	CYP3A5
M6	498	21.2	2.3	3.2	1.6
M1	482	23.6	55.1	48.1	40.3
Parent	510	25.6	16.4	ND	ND
M3	498	32.0	13.3	8.8	19.8
M4	453	41.5	4.0	13.0	15.2
M5	438	43.0	2.5	26.9	23.0

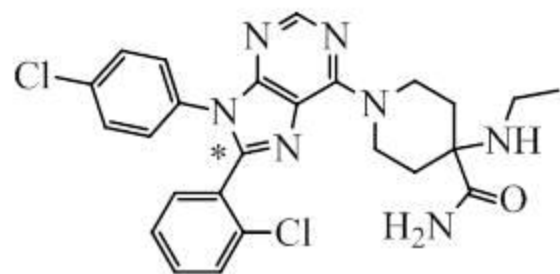
ND: not detected

DMD #43273

Table 6. Density functional calculations of the hydrogen atom abstraction energies (ΔE) of CP-945,598 and desethyl-CP-945,598 (M1) at marked carbon centers using the DFT/B3LYP 6-31G** method

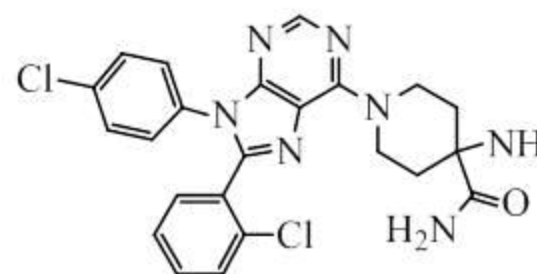
	Carbon Center	ΔE (kcal/mol)
	<i>a</i>	108.32
	<i>b</i>	97.24
	<i>c</i>	105.37
	<i>d</i>	97.71
	<i>M1-c</i>	105.06
	<i>M1-d</i>	98.00

* Absolute energies of CP-945,598 and M1 are -2346.6367622 and -2268.0153713 hartree, respectively.

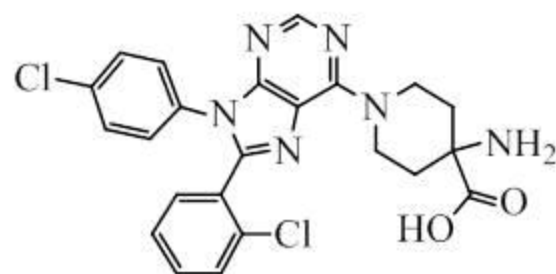


CP-945,598

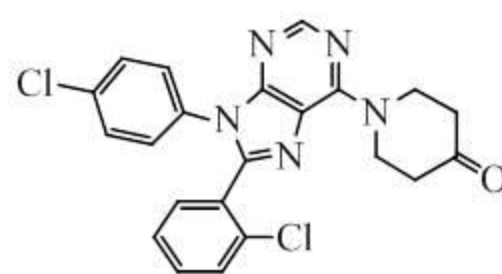
* site of ^{14}C -label



CE-156,706, M1



CE-114,764, M2



CE-127,773, M5

Fig. 1

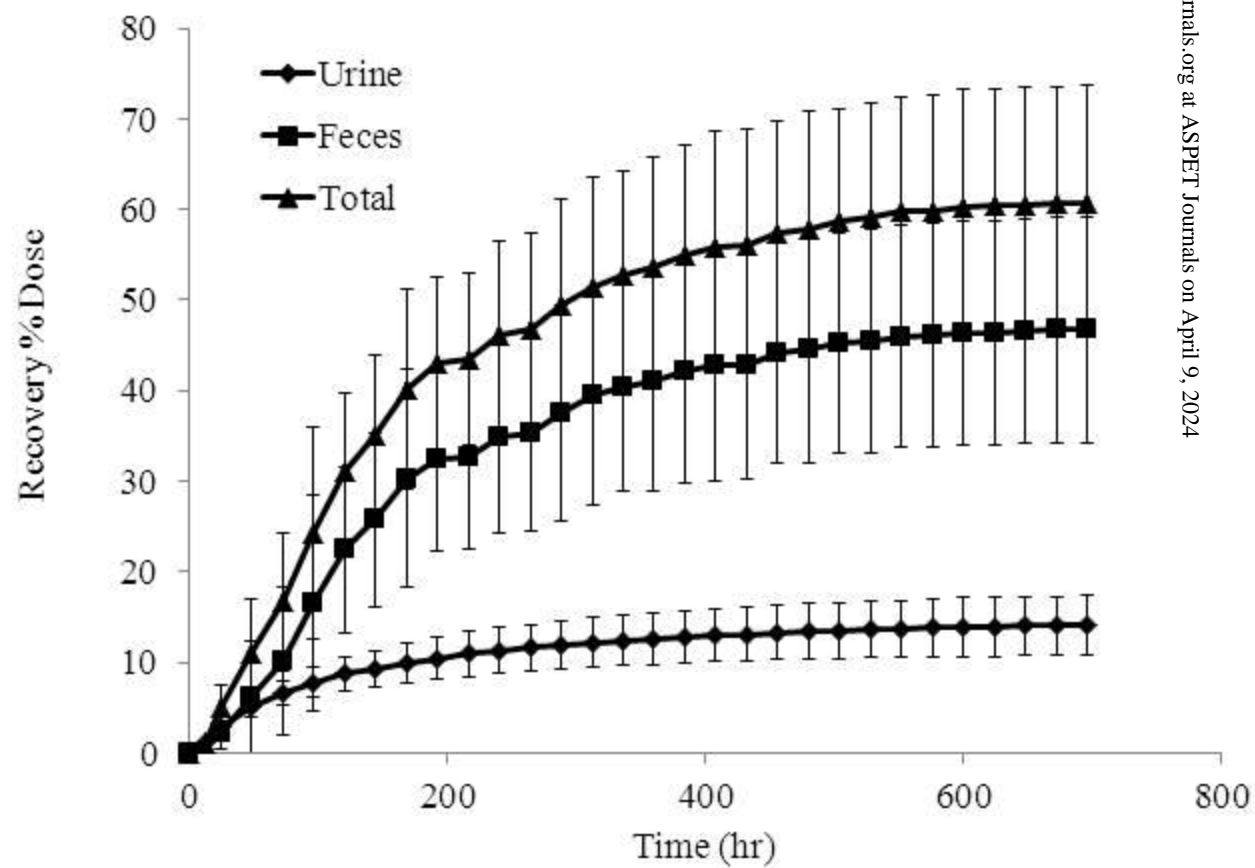


Fig.2

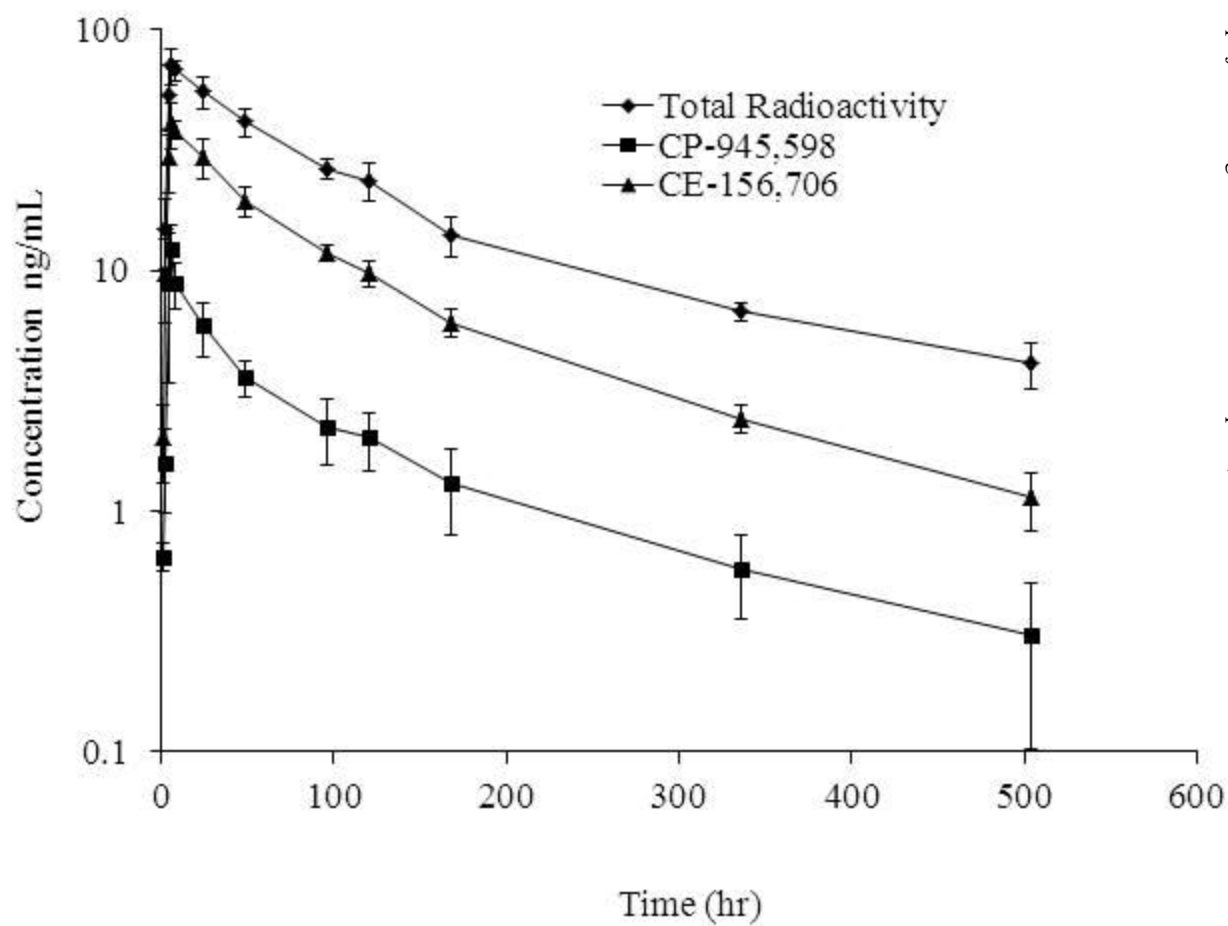


Fig. 3

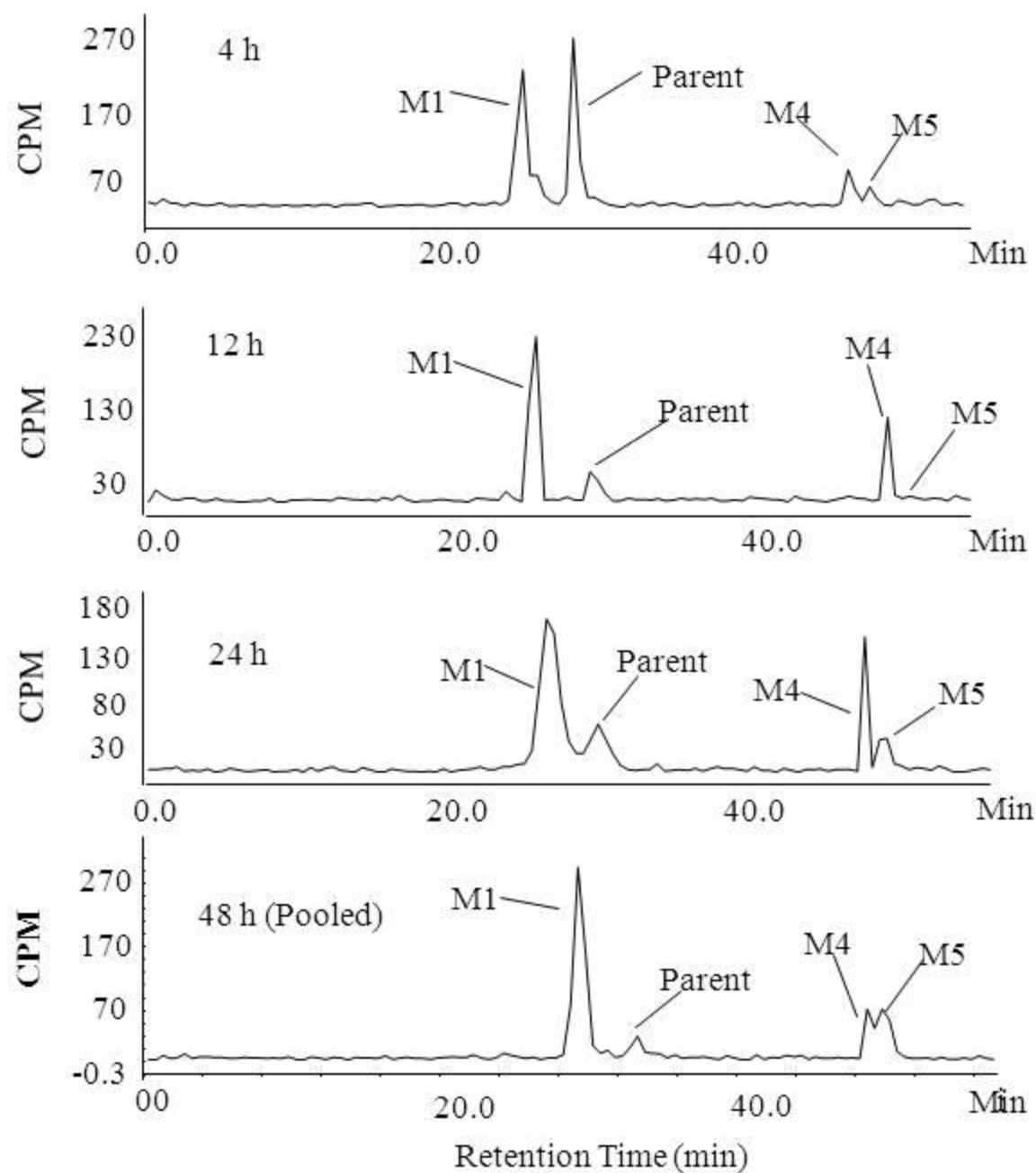


Fig. 4

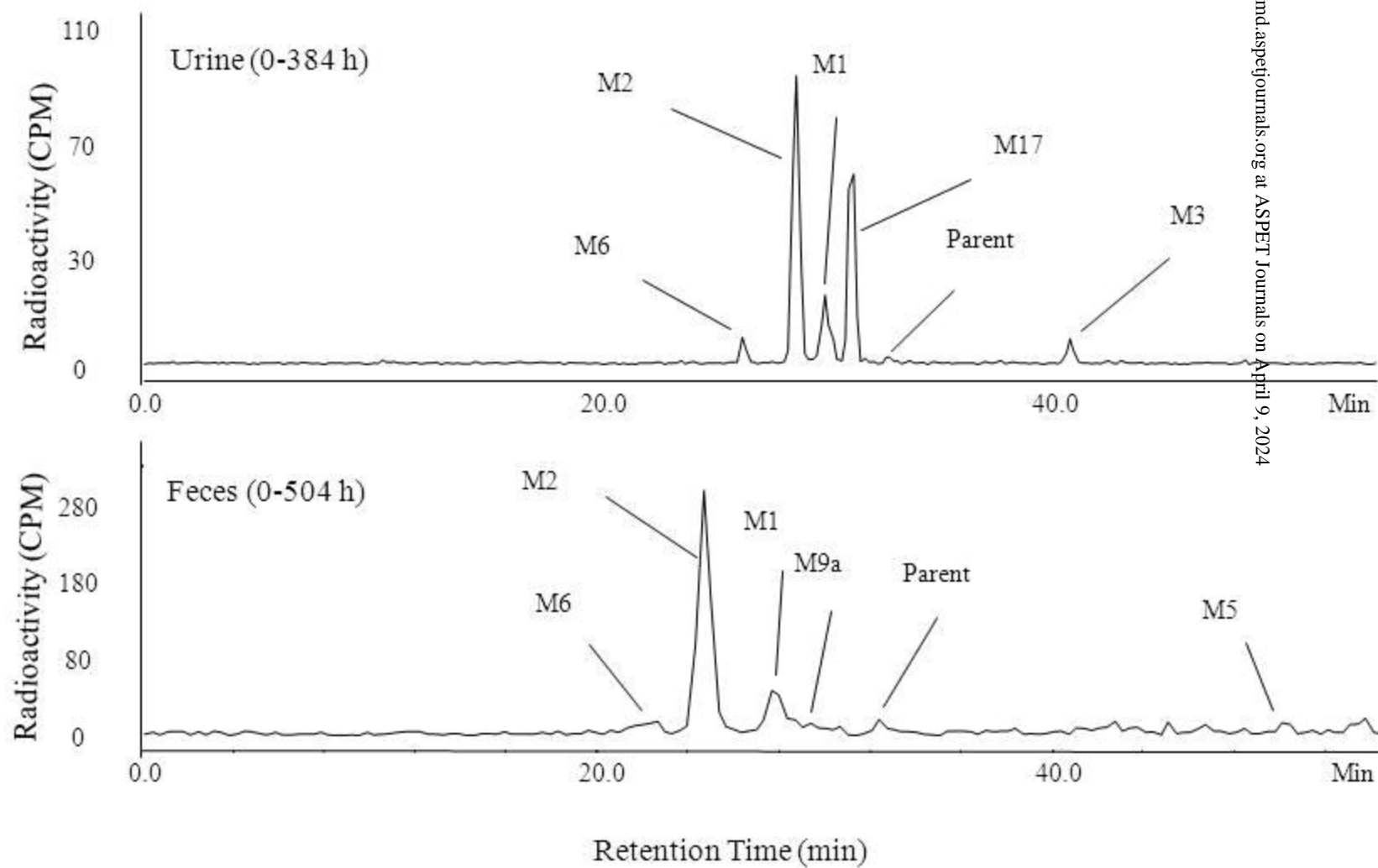


Fig.5

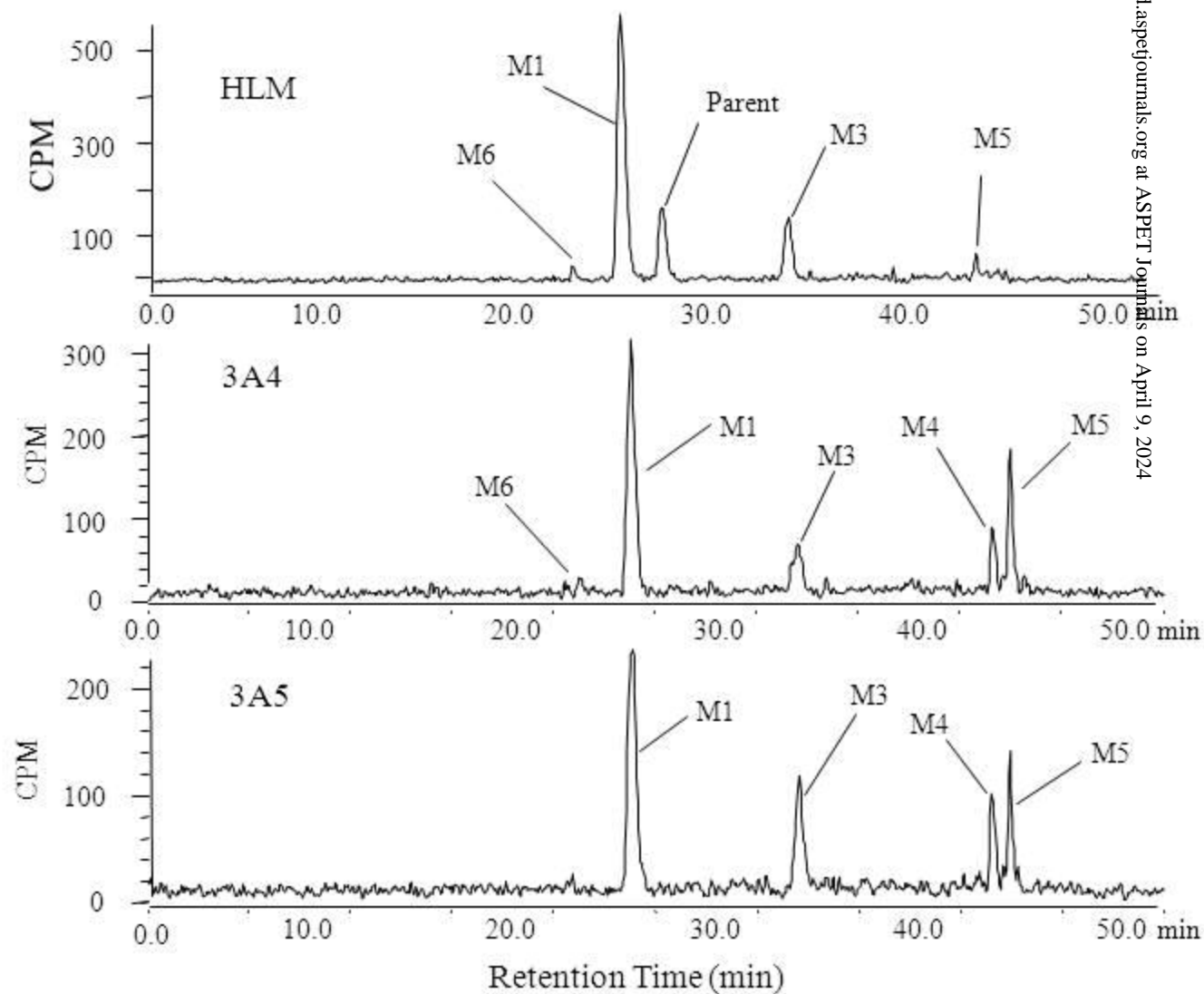


Fig. 6

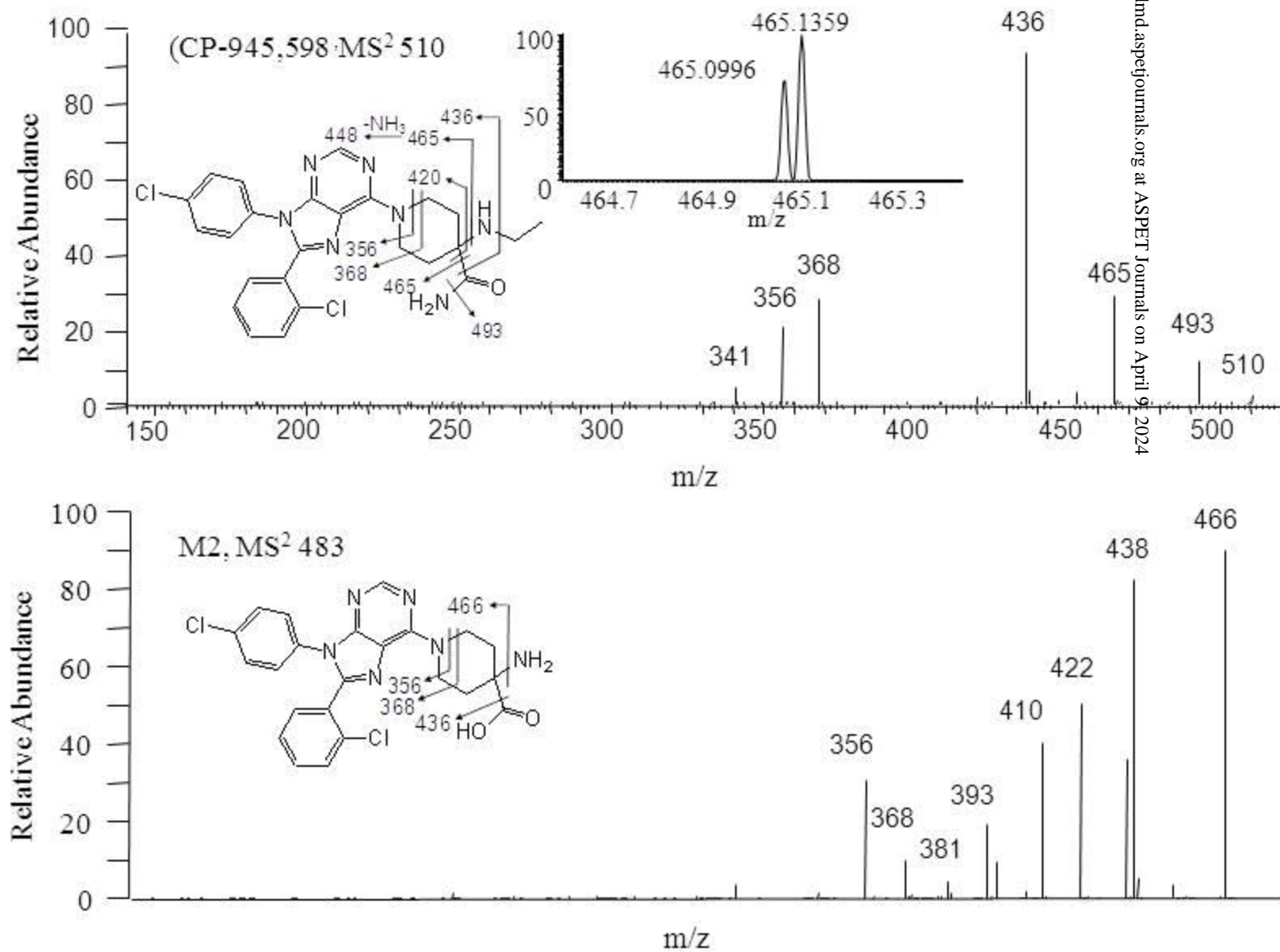


Fig. 7

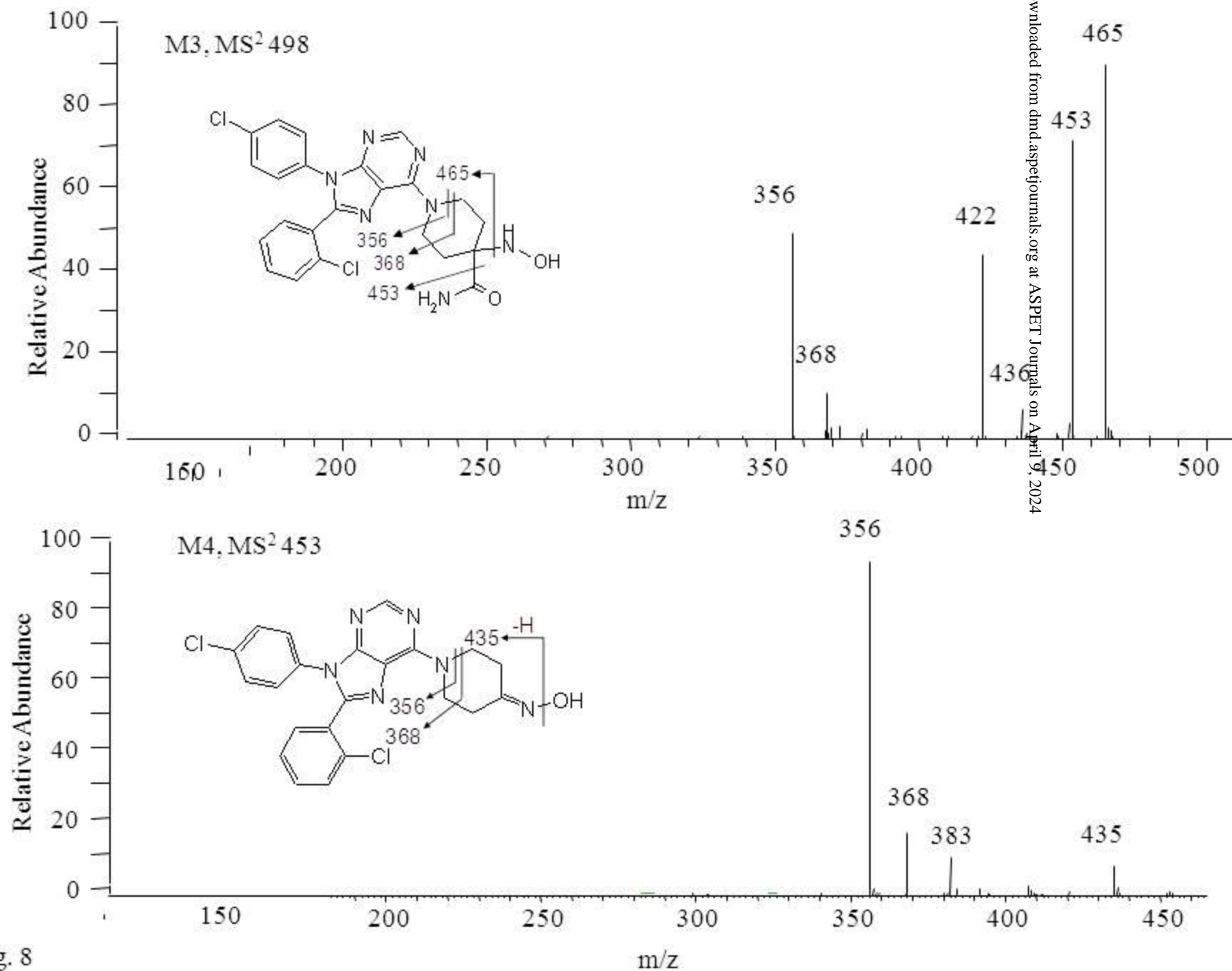


Fig. 8

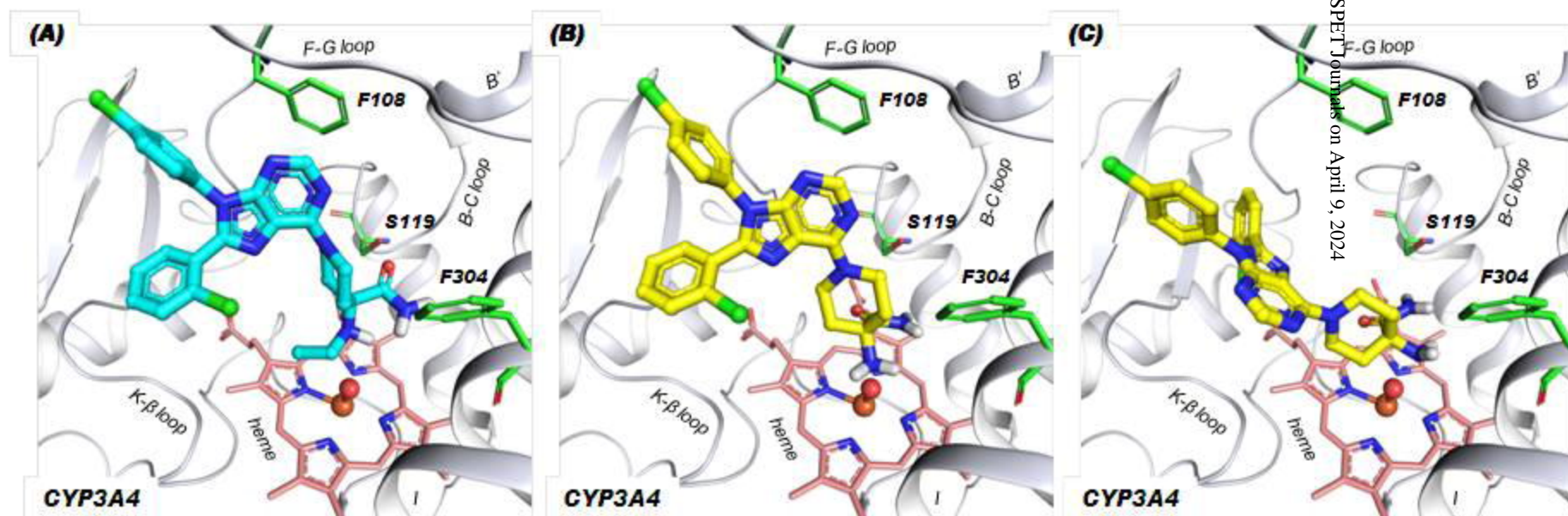


Fig. 9

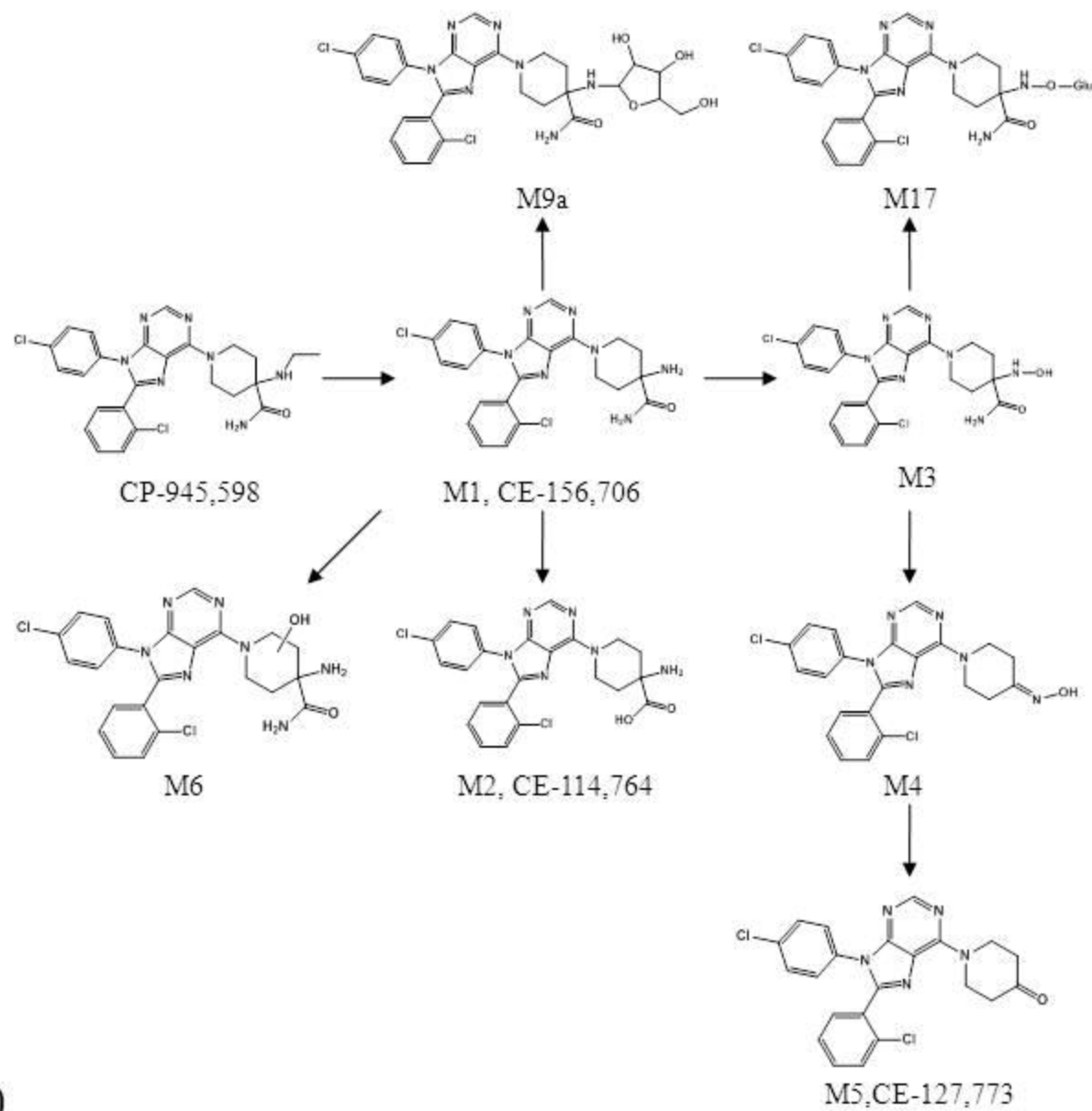


Fig 10